

Review

# Lithium Silicates in Anode Materials for Li-Ion and Li Metal Batteries

Yu-Sheng Su <sup>1,2,\*</sup>, Kuang-Che Hsiao <sup>3</sup>, Pedaballi Sireesha <sup>1</sup> and Jen-Yen Huang <sup>1</sup>

<sup>1</sup> International College of Semiconductor Technology, National Yang Ming Chiao Tung University, 1001 University Road, Hsinchu 30010, Taiwan; pedaballi.sireesha90@gmail.com (P.S.); rena0127@gmail.com (J.-Y.H.)

<sup>2</sup> Industry Academia Innovation School, National Yang Ming Chiao Tung University, 1001 University Road, Hsinchu 30010, Taiwan

<sup>3</sup> SYNergy ScienTech Corp., 6F-3, No. 9, Prosperity 1st Road, Hsinchu Science Park, Hsinchu 30078, Taiwan; shinehsiao1979@gmail.com

\* Correspondence: yushengsu@nycu.edu.tw

**Abstract:** The structural and interfacial stability of silicon-based and lithium metal anode materials is essential to their battery performance. Scientists are looking for a better inactive material to buffer strong volume change and suppress unwanted surface reactions of these anodes during cycling. Lithium silicates formed in situ during the formation cycle of silicon monoxide anode not only manage anode swelling but also avoid undesired interfacial interactions, contributing to the successful commercialization of silicon monoxide anode materials. Additionally, lithium silicates have been further utilized in the design of advanced silicon and lithium metal anodes, and the results have shown significant promise in the past few years. In this review article, we summarize the structures, electrochemical properties, and formation conditions of lithium silicates. Their applications in advanced silicon and lithium metal anode materials are also introduced.



**Citation:** Su, Y.-S.; Hsiao, K.-C.; Sireesha, P.; Huang, J.-Y. Lithium Silicates in Anode Materials for Li-Ion and Li Metal Batteries. *Batteries* **2022**, *8*, 2. <https://doi.org/10.3390/batteries8010002>

Academic Editor: Torsten Brezesinski

Received: 26 September 2021

Accepted: 28 December 2021

Published: 4 January 2022

**Publisher's Note:** MDPI stays neutral with regard to jurisdictional claims in published maps and institutional affiliations.



**Copyright:** © 2022 by the authors. Licensee MDPI, Basel, Switzerland. This article is an open access article distributed under the terms and conditions of the Creative Commons Attribution (CC BY) license (<https://creativecommons.org/licenses/by/4.0/>).

**Keywords:** silicon monoxide; silicon; metallic lithium; anode; energy storage; protective layer; volume expansion

## 1. Introduction

Silicon monoxide (SiO) is regarded as one of the next-generation anode materials to replace graphite in Li-ion batteries (LIBs). The advantages of SiO include low cost and abundant raw materials (silicon and silica), environmental benignity, facile fabrication, and high specific capacity (2100 mAh g<sup>-1</sup>) [1]. However, low conductivity, swelling after lithiation, and poor first-cycle efficiency (<60%) [2] in LIBs hinder the commercialization of SiO anodes. Researchers have designed the SiO anode material structure, majorly decorated with conductive carbon coatings, to boost the battery performance of SiO anodes in order to obtain high energy density, rapid charge/discharge capability, long cycle life, and improved first-cycle efficiency.

Current commercial SiO materials in the battery market are employed in anodes for LIBs and optical coating applications. SiO is synthesized by mixing silicon and silica in a 1:1 molar ratio and then subliming the mixture to collect the amorphous SiO (a-SiO) material. Since the silicon atoms in a-SiO are randomly distributed, their valence numbers can be 0, 1+, 2+, 3+, and 4+ upon the bonding condition with different numbers of oxygen atoms [3]. Some silicon atoms agglomerate and form tiny silicon crystals surrounded by other amorphous substances, with Si–O bonds that have different valence numbers of silicon. In LIBs, these tiny silicon crystals in a-SiO react with Li<sup>+</sup> ions and form Li<sub>15</sub>Si<sub>4</sub> [4,5], serving as the active material to store energy. Owing to the nano scale of tiny silicon crystal, no pulverization occurs after lithiation [6]; therefore, good reversibility can be obtained. The Si–O bonding area has more complicated reactions with Li<sup>+</sup> ions. Not only is a portion

of silicon reduced, forming lithium silicide alloys, but  $\text{Li}_2\text{O}$  and various lithium silicates can be formed, serving as ionic conductors and structural stabilizers [4,5].

Compared to  $\text{SiO}$  anode materials, high-capacity anode materials consisting of pristine silicon still have a lot of obstacles to be overcome due to their severe swelling behavior and poor cycle life [7,8]. Under systematic electrochemical characterizations,  $\text{SiO}$  anode outperformed silicon in terms of volume-expansion control, rate performance, and Li-diffusion coefficient [9]. It is believed that lithium silicates generated in situ in  $\text{SiO}$  anodes after initial lithiation play a critical role in buffering the volume expansion and maintaining structural integrity, resulting in great cycle performance comparable to conventional graphite anodes. There are also many recent publications showing that lithium silicates can serve as a good protective layer to improve battery performance of silicon-based and lithium metal anode materials. In this review, we introduce the material properties of different types of lithium silicates and their applications, as well as future prospects in anode materials for high-energy-density batteries.

## 2. Structures of Lithium Silicates

Before studying the structures of lithium silicates, we should understand how they are formed in lithiated a- $\text{SiO}$  material. Atomic models of suboxide-type tetrahedra in a- $\text{SiO}$  and amorphous  $\text{SiO}_2$  using angstrom-beam electron diffraction (ABED) and synchrotron high-energy XRD (HEXRD) techniques can be seen in Figure 1a,b [10], where a- $\text{SiO}$  exhibits a very disordered structure. It was found that five bonding structures can be formed in a- $\text{SiO}$ , including  $\text{Si}-4\text{Si}$ ,  $\text{Si}-(3\text{Si}+1\text{O})$ ,  $\text{Si}-(2\text{Si}+2\text{O})$ ,  $\text{Si}-(1\text{Si}+3\text{O})$ , and  $\text{Si}-4\text{O}$  (Figure 1c). This shows that pure silicon ( $\text{Si}-4\text{Si}$ ) and silica ( $\text{Si}-4\text{O}$ ) are not the only phases, but there are considerable fractions of various suboxide tetrahedra remaining in the interface of  $\text{Si}/\text{SiO}_2$ , leading to more complex reactions during lithiation/delithiation in LIBs. Since a- $\text{SiO}$  is a thermally unstable material, the disproportionation reaction transforms a- $\text{SiO}$  into a mixture of crystalline silicon and silica after heat treatments [11,12]. When disproportionated, a- $\text{SiO}$  is lithiated and delithiated, also showing distinctive behavior compared to pristine a- $\text{SiO}$ . As a result, owing to the variety of Si-O bonding structures, different lithium silicates could be generated in  $\text{SiO}/\text{SiO}_x$  anode materials after lithiation.

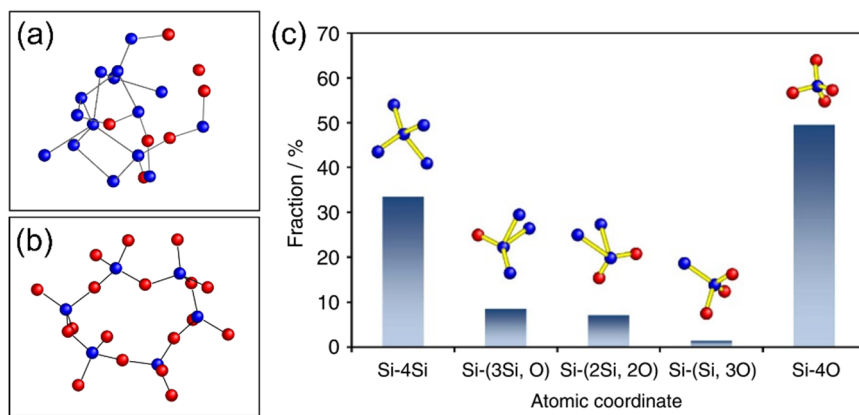


**Figure 1.** Atomic models of (a) interfacial suboxide-type tetrahedra in a- $\text{SiO}$  and (b) amorphous  $\text{SiO}_2$  in a- $\text{SiO}$ . (c) Fractions of the five atomic coordinates found in a- $\text{SiO}$ . The silicon atom is in blue, and the oxygen atom is in red. Reproduced with permission from ref. [10]. Copyright 2015, Nature Publishing Group.

Jung et al. adopted Vienna Ab Initio Simulation Package (VASP) to simulate lithiated  $\text{SiO}$  structure via density functional theory (DFT), Perdew-Burke-Ernzerhof (PBE), and projector-augmented wave (PAW) methods [13]. Figure 2 shows the possible phases composed of elements Li, Si, and O after the lithiation of  $\text{SiO}$ . In fact, not only can  $\text{Li}_4\text{SiO}_4$  proposed by a simple lithiation model [4] be generated, but crystalline  $\text{Li}_2\text{Si}_2\text{O}_5$  and  $\text{Li}_6\text{Si}_2\text{O}_7$  could also exist during the electrochemical reactions. When the ratio of Li to  $\text{SiO}$

is lower (2.65–3.54),  $\text{Li}_2\text{Si}_2\text{O}_5$  and  $\text{Li}_6\text{Si}_2\text{O}_7$  phases are generated. When the ratio of Li to  $\text{SiO}$  reaches more than 3.81, crystalline  $\text{Li}_4\text{SiO}_4$  is the dominant lithium silicate phase. In  $\text{Li}_2\text{Si}_2\text{O}_5$  and  $\text{Li}_6\text{Si}_2\text{O}_7$  structures, each  $\text{SiO}_4$  tetrahedron shares three oxygens and one oxygen with the neighboring tetrahedra, respectively, to form bonds. In contrast, the  $\text{SiO}_4$  tetrahedron of  $\text{Li}_4\text{SiO}_4$  does not share any oxygen. Due to the high activation energy of  $\text{SiO}_4$  tetrahedron decomposition,  $\text{Li}_2\text{Si}_2\text{O}_5$ ,  $\text{Li}_6\text{Si}_2\text{O}_7$ , and  $\text{Li}_4\text{SiO}_4$  are difficult to reduce to silicon or to convert into  $\text{Li}_2\text{O}$ , representing their high irreversibility [13].

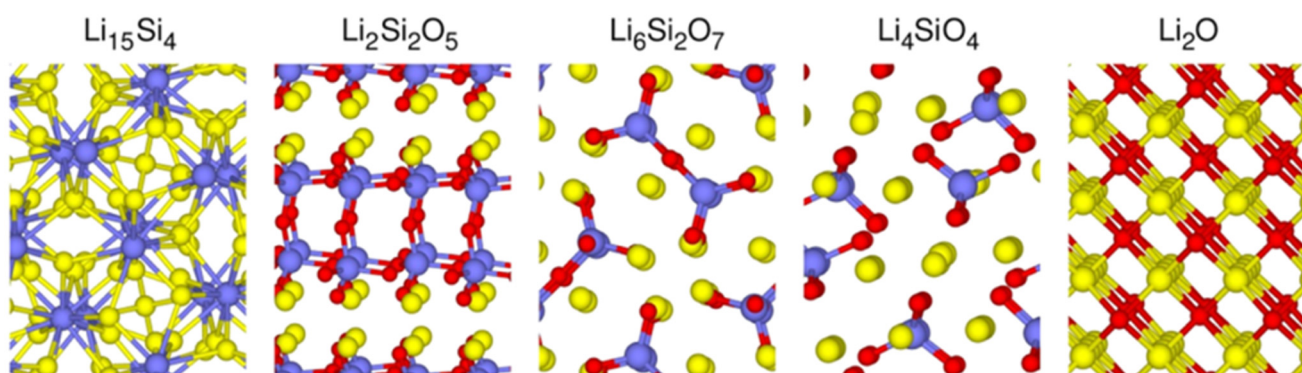
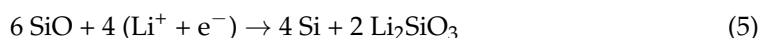
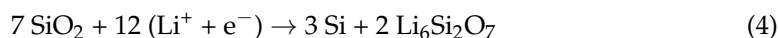
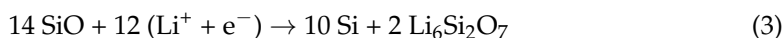


**Figure 2.** Crystalline structures of  $\text{Li}_{15}\text{Si}_4$ ,  $\text{Li}_2\text{Si}_2\text{O}_5$ ,  $\text{Li}_6\text{Si}_2\text{O}_7$ ,  $\text{Li}_4\text{SiO}_4$ , and  $\text{Li}_2\text{O}$ . The silicon atom is in blue, the oxygen atom is in red, and the lithium atom is in yellow. The bond length of Si-Si is 2.8 Å, and that of Si-O is 2.0 Å. To make the structures look succinct, only Si-O bonds are shown in  $\text{Li}_2\text{Si}_2\text{O}_5$ ,  $\text{Li}_6\text{Si}_2\text{O}_7$ , and  $\text{Li}_4\text{SiO}_4$ . Reproduced with permission from ref. [13]. Copyright 2015, ACS Publications.

### 3. Electrochemical Properties and Formation Conditions of Lithium Silicates

Since various lithium silicates have different crystalline structures and Li/Si ratios, their material properties and electrochemical properties are not the same. For instance, the Li diffusivities of compounds consisting of lithium, silicon, and oxide were calculated via the climbing-image nudged elastic band (CI-NEB) method, and the diffusivities ranked from low to high are:  $\text{Li}_6\text{Si}_2\text{O}_7 (1.8 \times 10^{-12}) < \text{Li}_2\text{Si}_2\text{O}_5 (1.3 \times 10^{-11}) < \text{Li}_4\text{SiO}_4 (1.1 \times 10^{-10}) < \text{Li}_2\text{O} (1.8 \times 10^{-8}) < \text{Li}_{15}\text{Si}_4 (8.8 \times 10^{-6})$  [13]. According to the simulation results, fully-lithiated silicon has the highest diffusivity compared to all lithium silicates, and  $\text{Li}_2\text{O}$  has a Li diffusivity that is two orders of magnitude higher than that of other inactive lithium silicates [13]. Another report demonstrated that at low Li concentrations, the diffusivity of  $\text{Li}^+$  ions in lithium silicates is two orders of magnitude lower than that of lithium silicides ( $\text{Li}_x\text{Si}$ ), but it rapidly increases with increasing Li content [14]. Lithium silicates with high Li-ion diffusivity facilitate fast charge/discharge capability, high utilization of active materials, and low polarization/overpotential. In the subsections below, we introduce the electrochemical properties and formation conditions of lithium silicates in anode materials. Simplified formation mechanisms of lithium silicates from  $\text{SiO}$  and  $\text{SiO}_2$  can be shown as follows (assuming  $\text{Li}_x\text{Si}_y\text{O}_z$  species are generated before  $\text{Li}_x\text{Si}$ ) [15,16]:





### 3.1. *Li<sub>4</sub>SiO<sub>4</sub>*

As one of the major phases in lithiated a-SiO, Li<sub>4</sub>SiO<sub>4</sub> is the most studied buffer material that minimizes the volume expansion of SiO anode [4,5,11,17]. Li<sub>4</sub>SiO<sub>4</sub> functions as an inactive material but can maintain structural integrity due to its strong mechanical strength. The capability of conducting Li<sup>+</sup> ions is very important for Li<sub>4</sub>SiO<sub>4</sub> to serve as both an ionic conductor and a buffer material, which guarantees smooth electrochemical reactions. It was reported that, in terms of Li ionic conductivity, the conductivity of crystalline Li<sub>4</sub>SiO<sub>4</sub> in SEI detected by atomic visualization is estimated to be 1000 times greater than that of Li<sub>2</sub>O, according to molecular dynamic simulation [18]. Pristine Li<sub>4</sub>SiO<sub>4</sub> has been identified as either chemically or electrochemically inactive with lithium [1]. This means that Li<sub>4</sub>SiO<sub>4</sub> can be neither lithiated nor delithiated once formed [1,19,20]. However, Hirose et al. demonstrated that Li<sub>4</sub>SiO<sub>4</sub> can release Li<sup>+</sup> ions at a high potential (2.5 V vs. Li/Li<sup>+</sup>) [17,21]. Additionally, it is believed that Li<sub>4</sub>SiO<sub>4</sub> is the lithium silicate with the highest Li/Si ratio that can be formed in an electrochemical cell. Coyle et al. adopted radio-frequency magnetron sputtering of both SiO<sub>2</sub> and Li<sub>2</sub>O targets to make thin lithium silicate films with various compositions, and a lithium-rich Li<sub>8</sub>SiO<sub>6</sub> (Li/Si = 8) phase was confirmed by inductively coupled optical emission spectrometry (ICP-OES), Fourier transform infrared (FTIR) spectroscopy, time-of-flight secondary-ion mass spectrometry (ToF-SIMS), and X-ray photoelectron spectroscopy (XPS) [22]. However, there have been no electrochemical performance data reported on Li-rich lithium silicates with a Li/Si ratio higher than four.

Yamamura et al. found that neither crystalline Li<sub>4</sub>SiO<sub>4</sub> nor SiO<sub>2</sub> can react with lithium metal, but amorphous SiO<sub>2</sub> showed Li-ion activity [1]. It is believed that the SiO<sub>4</sub> tetrahedra in Li<sub>4</sub>SiO<sub>4</sub> and SiO<sub>2</sub> are difficult to reduce by lithium metal and ions, but the dangling bonds and distorted SiO<sub>4</sub> tetrahedra in a-SiO<sub>2</sub> can facilitate reactions with lithium. The formation energy (E<sub>f</sub>) of lithium inserting into the SiO<sub>4</sub> tetrahedra of crystalline SiO<sub>2</sub> can be calculated. When lithium stays in the O vacancy (Figure 3a), the E<sub>f</sub> is 0.44 eV, requiring extra energy to be stabilized. When lithium is in the Si vacancy (Figure 3b), the E<sub>f</sub> is −3.66 eV, which represents a spontaneous exothermic reaction of Li<sup>+</sup> with O<sup>−</sup>. This indicates that lithium has a high tendency to bond with oxygen due to the electrostatic attraction force originating from their opposite charges. In addition, when lithium is located at the empty sites in the structure shown in Figure 3c,d, the E<sub>f</sub> is 1.15 eV and 1.18 eV, respectively, implying the difficulty of creating bonds. Sivonxay et al. employed DFT and ab initio molecular dynamics (AIMD) methods to demonstrate that amorphous SiO<sub>2</sub> is thermodynamically driven to be lithiated, which shows that Li–O local environments are increasingly favored, as compared to Si–O bonding [14]. Moreover, amorphous SiO<sub>2</sub> and SiO have disordered structures, including many vacancies, dangling bonds, and non-equivalent bond lengths, offering more reaction sites for lithiation. This explains why amorphous silicon oxides exhibit lithium activity, while crystalline Li<sub>4</sub>SiO<sub>4</sub> and SiO<sub>2</sub> are considered chemically and electrochemically inert with lithium.

Lithium silicates were also discovered in the oxidized surface of silicon nanoparticles during cycling in LIBs [23]. When pure silicon is in contact with air, a thin nanocoating of silica is formed on the silicon surface, which prevents further oxidation. Figure 4 exhibits how the microstructure and composition of nano-sized Si with naturally formed SiO<sub>2</sub> change, along with discharge and charge conditions. When the silica-covered silicon anode is discharged to ~0.5 V, a solid electrolyte interface (SEI) layer is formed under the electrolyte reduction reactions. This layer passivates the anode surface to avoid further Li-ion and electrolyte consumption. While the Li/Si cell is deeply discharged, both Li<sub>x</sub>Si<sub>y</sub>O<sub>x</sub> and Li<sub>2</sub>O are formed in the surface oxide region, and Li<sub>x</sub>Si is formed in the core silicon region. By analyzing the signal of Si 2p spectra, it was confirmed that Li<sub>4</sub>SiO<sub>4</sub> is the main lithium silicate phase [23]. After the cell is recharged to 0.9 V, Li<sub>2</sub>O is gone, but Li<sub>4</sub>SiO<sub>4</sub> still exists in the structure, evidencing the reversibility of Li<sub>2</sub>O and the irreversibility of Li<sub>4</sub>SiO<sub>4</sub>. On the

surface of a silicon anode,  $\text{Li}_4\text{SiO}_4$  remains in the protective layer, remaining unchanged during cycling, similar to a-SiO and disproportionated  $\text{SiO}_x$  anodes [12,13].

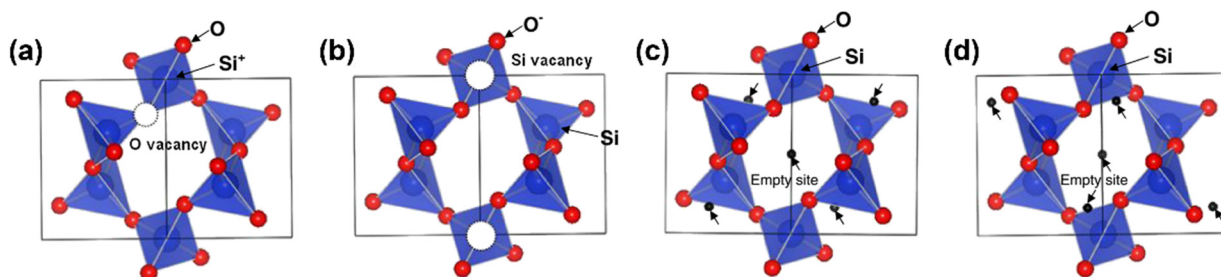


**Figure 3.** The crystalline structure of  $\text{SiO}_2$  ( $P3121$  space group) drawn via the VESTA method (a) with O vacancy, (b) with Si vacancy, and (c,d) with empty sites. Reproduced with permission from ref. [1]. Copyright 2011, The Ceramic Society of Japan.

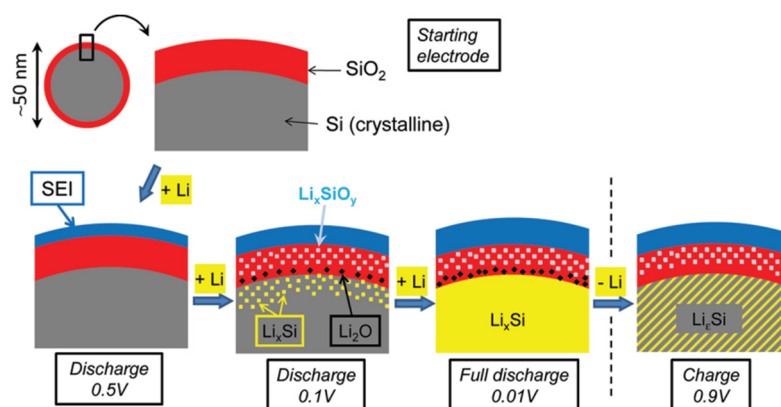


**Figure 4.** Microstructure of nano-sized Si with naturally formed  $\text{SiO}_2$  on the surface. Composition changes during shallow and deep discharge and full recharge. Reproduced with permission from ref. [23]. Copyright 2012, ACS Publications.

The formation of  $\text{Li}_4\text{SiO}_4$  in  $\text{SiO}/\text{SiO}_x$ -based anodes occurs during the first discharge process at  $<0.24$  V vs.  $\text{Li}/\text{Li}^+$ , and the crystalline phase remains in the anode structure regardless of cell recharge or cycling, showing strong irreversibility [19,20,24]. Besides the electrochemically generated  $\text{Li}_4\text{SiO}_4$  in situ,  $\text{Li}_4\text{SiO}_4$  can be synthesized by the thermal reaction of  $\text{SiO}$  and lithium hydroxide cofired at  $550$  °C [25,26]. A simple hydrothermal synthesis method ( $175$  °C) using fumed silica and lithium hydroxide can also produce  $\text{Li}_4\text{SiO}_4$  [27]. A citric-acid-based sol-gel route (also with fumed silica and  $\text{LiOH}$ ) was developed to synthesize macroporous  $\text{Li}_4\text{SiO}_4$  with a carbon coating [28]. Due to the stability of electrochemical cells and the synthesizability of  $\text{Li}_4\text{SiO}_4$ , it can serve as a promising protective buffer material for silicon and lithium metal anodes, which will be discussed in the next section.

### 3.2. $\text{Li}_2\text{SiO}_3$

$\text{Li}_2\text{SiO}_3$  has lithium activity, unlike  $\text{Li}_4\text{SiO}_4$ , with a reversible capacity of  $<200$  mA h g<sup>-1</sup> [29]. Yang et al. utilized graphene to prepare a composite material with  $\text{Li}_2\text{SiO}_3$  as the anode, showing good cycle life [29]. Pristine  $\text{Li}_2\text{SiO}_3$  has sloping charge/discharge curves with an average voltage above  $1$  V, and it can be reversibly cycled in a half cell with lithium metal.  $\text{Li}_2\text{SiO}_3$  can be formed by heating a graphite/ $\text{Li}_4\text{SiO}_4$  mixture at  $600$  °C [30]. A graphite composite sample with  $\text{Li}_2\text{SiO}_3$  obtained a higher capacity than that with  $\text{Li}_4\text{SiO}_4$ , although larger first-cycle capacity loss was also found in an anode sample with  $\text{Li}_2\text{SiO}_3$ . Xiao et al. pointed out that  $\text{Li}_2\text{SiO}_3$  can improve Li-ion diffusion behavior

for better rate performance and that co-existing  $\text{Li}_2\text{CO}_3$  favors the growth of a denser and more conductive SEI layer [30].  $\text{Li}_2\text{SiO}_3$  has also been synthesized in a graphene composite material with  $\text{Li}_4\text{Ti}_5\text{O}_{12}$  or  $\text{Li}_2\text{SnO}_3$  [31,32]. Both anode composite materials with  $\text{Li}_2\text{SiO}_3$  have better capacity and rate performance due to their lithium activity and good ionic conductivity.

$\text{Li}_2\text{SiO}_3$  was also found in lithiated  $\text{SiO}/\text{SiO}_x$ -based anode materials and electrodes under both shallow and deep lithiation conditions [1,33,34]. Both  $\text{Li}_4\text{SiO}_4$  and  $\text{Li}_2\text{SiO}_3$  can be generated either by chemical lithiation with lithium foil or powder at  $600\text{ }^\circ\text{C}$ – $800\text{ }^\circ\text{C}$  (Figure 5a) or electrochemical lithiation within a half cell with a lithium metal. Since  $\text{Li}_4\text{SiO}_4$  is an inert material for lithiation/delithiation and  $\text{Li}_2\text{SiO}_3$  is active to  $\text{Li}^+$  ions with good reversibility, there should be reversible phases of Li-rich compounds formed after  $\text{Li}_2\text{SiO}_3$  lithiation, which have not yet been identified. Wang et al. claimed that  $\text{Li}_2\text{SiO}_3$  reacts with  $\text{Li}^+$  ions and generates  $\text{Li}_2\text{O}$  and Si [32], but this claim needs further confirmation.

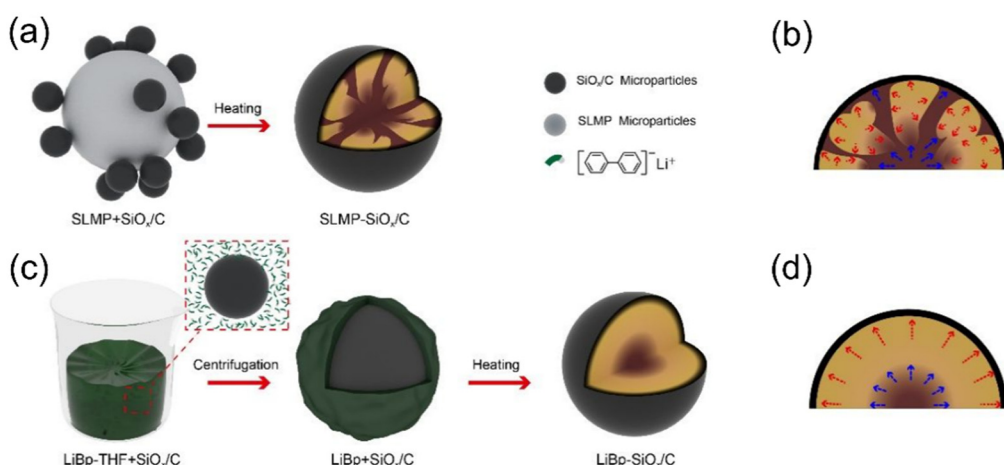


**Figure 5.** Schematic drawing illustrating the synthesis process and internal stresses for (a,b) SLMP- $\text{SiO}_x/\text{C}$  and (c,d)  $\text{LiBp-}\text{SiO}_x/\text{C}$ . Reproduced with permission from ref. [34]. Copyright 2020, ACS Publications.

Other than being generated *in situ* in electrochemical cells or via chemical lithiation processes with lithium metal,  $\text{Li}_2\text{SiO}_3$  can be synthesized by using the hydrothermal method followed by a heat process [29,31,32]. First, silicon and  $\text{LiOH}$  are well mixed in a Teflon-lined autoclave and heated at  $180\text{ }^\circ\text{C}$  for an appropriate dwell time, and then the product is transferred to a furnace under inert gas and sintered at  $600\text{ }^\circ\text{C}$ – $800\text{ }^\circ\text{C}$ ; as a result, pure  $\text{Li}_2\text{SiO}_3$  can be obtained [29]. Hydrothermal synthesis using  $\text{H}_2\text{SiO}_3$  as the starting material instead of silicon can also produce  $\text{Li}_2\text{SiO}_3$  without post-heat treatments [35]. A few studies have reported that  $\text{Li}_2\text{SiO}_3$  and byproduct  $\text{Li}_2\text{CO}_3$  can be formed when  $\text{Li}_4\text{SiO}_4$  reacts with  $\text{CO}_2$  gas [28,30]. A water-based sol-gel method adopting fumed silica and  $\text{LiOH}$  can produce  $\text{Li}_2\text{SiO}_3$  and  $\text{Li}_2\text{CO}_3$  at  $500\text{ }^\circ\text{C}$ , but  $\text{Li}_4\text{SiO}_4$  is the only dominant phase if the intermediate is heated up to  $675\text{ }^\circ\text{C}$  [36]. Obviously,  $\text{Li}_2\text{SiO}_3$  and  $\text{Li}_4\text{SiO}_4$  are mutually convertible when  $\text{Li}_2\text{CO}_3$  or  $\text{CO}_2$  is introduced into the thermal process.

### 3.3. $\text{Li}_2\text{Si}_2\text{O}_5$

$\text{Li}_2\text{Si}_2\text{O}_5$  was found as a result of characterizations of selected-area electron diffraction (SAED) under high-resolution transmission electron microscopy (HRTEM) with other lithium silicates ( $\text{Li}_4\text{SiO}_4$  and  $\text{Li}_6\text{Si}_2\text{O}_7$ ) in an  $\text{NaOH}$ -etched  $\text{SiO}$  anode during electrochemical lithiation and delithiation [20]. All three lithium silicates were preserved, even when the Li metal half cell was discharged to  $0\text{ V}$  [19,20].  $\text{Li}_2\text{Si}_2\text{O}_5$  should be the lithium silicate phase formed in the early stage because of its low  $\text{Li/Si}$  ratio. However, only  $\text{Li}_2\text{Si}_2\text{O}_5$  disappeared, while  $\text{Li}_4\text{SiO}_4$  and  $\text{Li}_6\text{Si}_2\text{O}_7$  remained after the cell was charged to  $2\text{ V}$ . It was proposed that  $\text{Li}_4\text{SiO}_4$  and  $\text{Li}_6\text{Si}_2\text{O}_7$  are irreversible phases in LIBs, but  $\text{Li}_2\text{Si}_2\text{O}_5$  can react with Si and then be converted into  $\text{SiO}_x$  during delithiation [19,20,37] or react with

additional  $\text{Li}^+$  ions to obtain  $\text{Li}_2\text{SiO}_3$  and Si [15]. Another paper reporting a thin  $\text{SiO}_2$  film electrode utilized in LIBs showed that the lithiated product  $\text{Li}_2\text{Si}_2\text{O}_5$  has good cyclability and can be converted back to  $\text{SiO}_2$  at 3.0 V vs.  $\text{Li}/\text{Li}^+$  [38]. Lener et al. calculated the free energy for the lithiation reaction of silica and concluded that  $\text{Li}_2\text{Si}_2\text{O}_5$  is, thermodynamically, the most favorable lithium silicate product [39].

In addition to hydrothermal synthesis [40],  $\text{Li}_2\text{Si}_2\text{O}_5$  was able to be synthesized using carbon-coated  $\text{SiO}_x$  ( $\text{SiO}_x/\text{C}$ ) microparticles and lithium-biphenyl (LiBp) complex solution, as shown in Figure 5c. In contrast to the lithiation method utilizing stabilized lithium metal power (SLMP) exhibited in Figure 5a, LiBp complex solution provides a homogeneous lithiation environment due to the intimate contact of  $\text{SiO}_x/\text{C}$  with the Li-containing solution. Chemical lithiation that adopts SLMP, usually in several microns, can only offer point-to-point lithiation channels where the particles are in contact with each other (Figure 5a). The relatively inhomogeneous lithiation leads to randomly distributed  $\text{Li}_x\text{Si}_y\text{O}_z$  formation, resulting in strong internal stresses and thereby pulverization (Figure 5b). The LiBp- $\text{SiO}_x/\text{C}$  sample has a uniform  $\text{Li}_2\text{Si}_2\text{O}_5$  coating on the particle; thereby, much better cycle performance and internal stress control can be obtained (Figure 5d). Yan et al. attributed the formation of  $\text{Li}_2\text{Si}_2\text{O}_5$  to the homogeneous absorption of LiBp on the  $\text{SiO}_x/\text{C}$  surface, which supports stable lithiation reactions, avoiding both excess and deficient lithium supply, as shown in the SLMP- $\text{SiO}_x/\text{C}$  sample processed by solid-state lithiation [34].

### 3.4. $\text{Li}_6\text{Si}_2\text{O}_7$

As mentioned above,  $\text{Li}_6\text{Si}_2\text{O}_7$  co-exists with  $\text{Li}_2\text{Si}_2\text{O}_5$  and  $\text{Li}_4\text{SiO}_4$  in  $\text{SiO}/\text{SiO}_x$ -based anodes during discharge and charge reactions [19,20]. Figure 6 explicitly displays the generation and transformation of lithium silicate phases at different delithiation and lithiation voltages [19]. At 0.4 V,  $\text{Li}_2\text{Si}_2\text{O}_5$  and  $\text{Li}_6\text{Si}_2\text{O}_7$  first appear in the anode, as shown in Figure 6b. When further discharged to 0.15 V, the porous  $\text{SiO}_x$  anode starts to generate  $\text{Li}_4\text{SiO}_4$ , and both  $\text{Li}_2\text{Si}_2\text{O}_5$  and  $\text{Li}_6\text{Si}_2\text{O}_7$  remain in the anode structure until 0 V (Figure 6c,d). All three lithium silicates can be still observed when the cell is charged to 0.4 V (Figure 6e), which is a higher charge than that of the formation voltage of  $\text{Li}_4\text{SiO}_4$ . At a full charge of 2 V (exhibited in Figure 6f)  $\text{Li}_2\text{Si}_2\text{O}_5$  disappears, but  $\text{Li}_6\text{Si}_2\text{O}_7$  and  $\text{Li}_4\text{SiO}_4$  cannot be delithiated and remain in the structure as the dominant phases.  $\text{Li}_6\text{Si}_2\text{O}_7$  is clearly an irreversible phase, like  $\text{Li}_4\text{SiO}_4$ , playing a role as a buffer material in  $\text{SiO}/\text{SiO}_x$ -based anodes to alleviate their swelling behavior. It is worth noting that a reversible  $\text{Li}_2\text{SiO}_3$  phase was not detected in the reports from the same research group [19,20,24], in contrast to the results of a later study [33]. A possible reason for this contradiction is that  $\text{Li}_2\text{SiO}_3$  may be formed at a very early stage of lithiation and synchronously converted into Si and  $\text{Li}_2\text{O}$  due to further lithiation [31,32].

There are no studies in the literature reporting successful synthesis of sole  $\text{Li}_6\text{Si}_2\text{O}_7$  as the only lithium silicate phase. In the previous studies,  $\text{Li}_6\text{Si}_2\text{O}_7$  was synthesized, along with other lithium silicates, such as  $\text{Li}_2\text{SiO}_3$  and  $\text{Li}_4\text{SiO}_4$  [41,42].  $\text{Li}_6\text{Si}_2\text{O}_7$  (15%) was produced with  $\text{Li}_2\text{SiO}_3$  (40%) and  $\text{Li}_4\text{SiO}_4$  (45%) by annealing a melt consisting of  $60\text{Li}_2\text{O} \cdot 40\text{SiO}_2$  prepared at 1250 °C [41]. Mixed lithium silicate phases including  $\text{Li}_6\text{Si}_2\text{O}_7$  as impurities were obtained in an LTAP ( $\text{Li}_{1.3}\text{Ti}_{1.7}\text{Al}_{0.3}(\text{PO}_4)_3$ ) sample with an  $\text{Li}_2\text{O}$  additive [43].  $\text{Li}_6\text{Si}_2\text{O}_7$  as a minor phase can also be synthesized with  $\text{Li}_4\text{SiO}_4$  using a sintering process of a  $\text{Li}_2\text{CO}_3$  and  $\text{SiO}_2$  mixture between 750 °C and 850 °C [42]. However, the  $\text{Li}_6\text{Si}_2\text{O}_7$  phase vanishes when the heating temperature is increased to 900 °C. It was reported that  $\text{Li}_6\text{Si}_2\text{O}_7$  is a metastable lithium silicate phase, which can be decomposed into  $\text{Li}_2\text{SiO}_3$  and  $\text{Li}_4\text{SiO}_4$  at a high temperature [44].

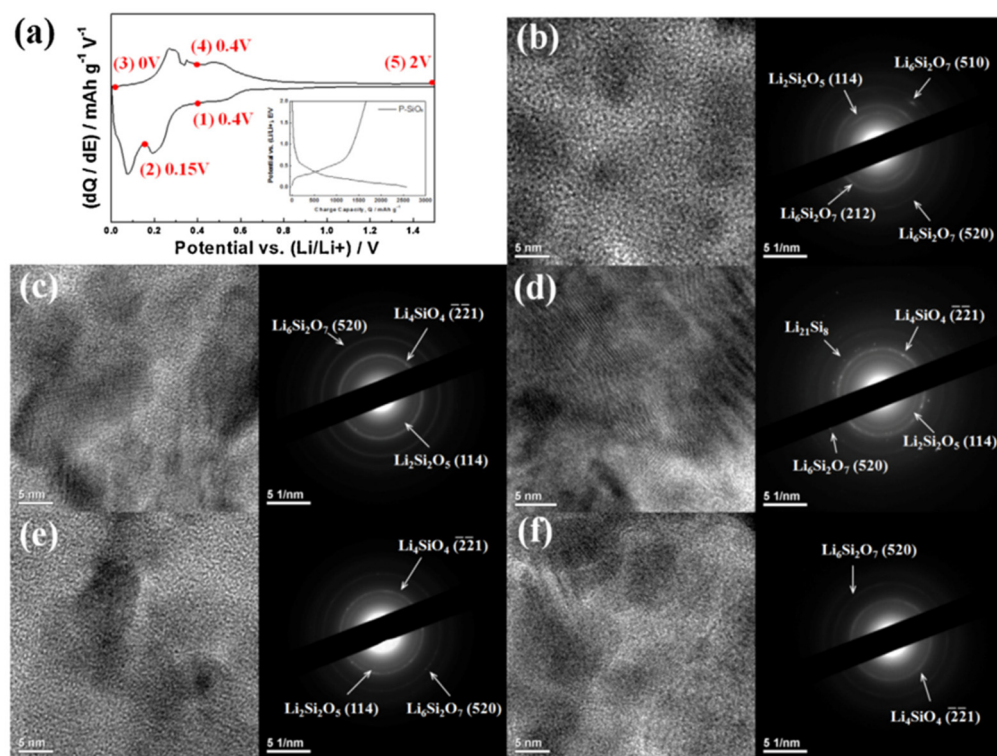


**Figure 6.** (a) Differential capacity plot (DCP) and charge/discharge profile of porous  $\text{SiO}_x$  anode at the first cycle. Ex situ HRTEM images with SAED patterns of porous  $\text{SiO}_x$  anode at various potentials indicated in DCP. (b) Discharge at 0.4 V, (c) discharge at 0.15 V, (d) discharge at 0 V, (e) charge at 0.4 V, and (f) charge at 2 V. Reproduced with permission from ref. [19]. Copyright 2013, Elsevier.

#### 4. Lithium Silicates in Silicon, Lithium Metal, and Other Anode Materials

The success of lithium silicates in  $\text{SiO}/\text{SiO}_x$ -based anodes has prompted researchers to investigate their use in high-capacity silicon and lithium metal anode systems. Both anodes have unsettled problems, such as dramatic volume change, unstable interfacial reactions, and poor cycle performance [45–49]. In a typical  $\text{SiO}$  anode, the lithium silicates formed in situ after the initial lithiation act as a rigid framework to accommodate the swelled  $\text{Li}_x\text{Si}$  alloy, and the lithium silicates in the structure can provide good ionic channels at the same time [11]. Figure 7 displays the common positional design of lithium silicates in  $\text{SiO}/\text{SiO}_x$ , nano-Si, and lithium metal anode materials. Both  $\text{SiO}$  and nano-Si are in powder form, but only  $\text{SiO}$  possesses a structure with dispersed lithium silicates. On the other hand, lithium silicates are usually applied as a coating layer in nano-Si and metallic lithium anodes. Methods of applying lithium silicates in anode structures have been extensively developed. Below, we give some examples of how to employ lithium silicates in order to stabilize the electrochemical reactions of silicon and lithium metal anode materials, thereby prolonging their cycle life.

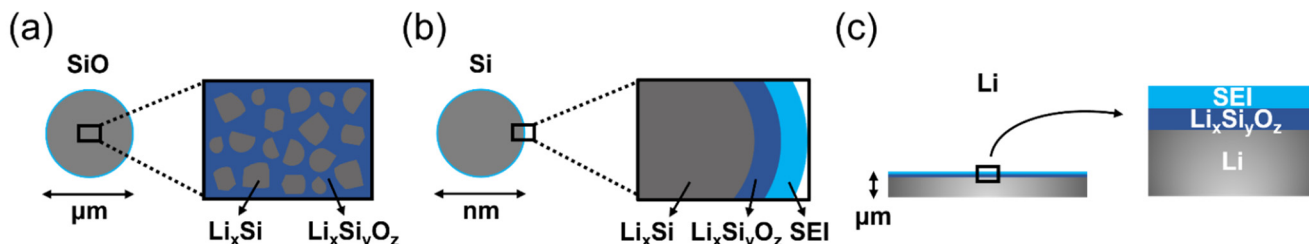


**Figure 7.** Schematic drawing illustrating the lithium silicates ( $\text{Li}_x\text{Si}_y\text{O}_z$ ) in the structure of (a)  $\text{SiO}/\text{SiO}_x$ , (b) nano-Si, and (c) metallic lithium anode materials.

#### 4.1. Lithium Silicates in Silicon Anodes

Cao et al. analyzed the composition of SEI formed on the native oxide-covered silicon anodes by employing *in situ* synchrotron X-ray reflectivity, linear sweep voltammetry, and *ex situ* XPS [16]. The inorganic SEI comprised two well-defined structures, which can be divided into a bottom SEI layer (adjacent to the electrode) and a top SEI layer (adjacent to the organic SEI layer from electrolyte decomposition), as shown in Figure 8. At open circuit voltage (OCV), the silicon surface is terminated by the pristine native silica (Figure 8A). While lithiation begins and the anode voltage drops to 0.8 V vs. Li/Li<sup>+</sup>, the organic SEI starts to form on the silicon anode, and native silica remains unchanged (Figure 8B). At 0.7 V, the lithiation of the native oxide layer initiates and transforms into lithium silicates ( $\text{Li}_x\text{SiO}_y$ ) [16,50,51] and lithium silicide alloys ( $\text{Li}_x\text{Si}$ ) as the bottom SEI layer (Figure 8C). This finding is also in consistent with another report, which concluded that the lithiation voltage of  $\text{SiO}_2$  is higher than that of Si [14]. Between 0.6 V and 0.3 V, the top SEI, consisting of LiF and other products, is formed in between the organic SEI and bottom SEI, and lithiation of the bottom SEI continues (Figure 8D). At 0.2 V, the last step of SEI formation,  $\text{Li}_2\text{O}$  is formed in the bottom SEI layer, which is thicker than the top SEI (Figure 8E). The authors concluded that a smooth  $\text{Li}_x\text{SiO}_y$  layer as the bottom SEI can secure the growth of a conformal, smooth, and thin top SEI layer, and both cycle stability and rate performance can be guaranteed [16]. It was reported that  $\text{Li}_4\text{SiO}_4$  should be the final lithium silicate product from the lithiation of either native oxide or artificial oxide grown on an Si surface, and a small lithiation current is necessary to activate the electrochemical synthesis of lithium silicates [23,52].

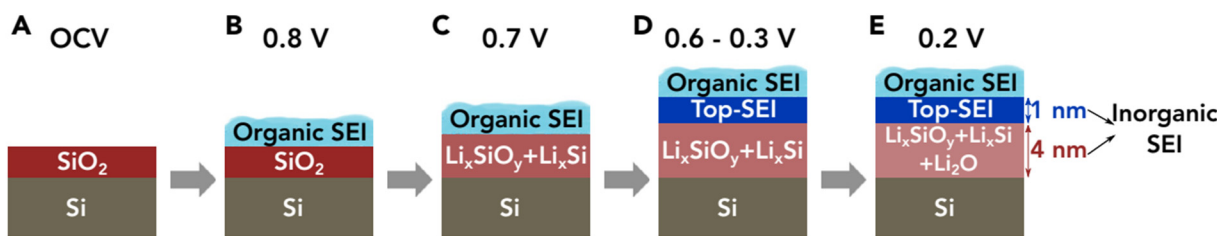


**Figure 8.** (A–E) Schematic drawing illustrating the proposed voltage-dependent SEI growth mechanism on native oxide-terminated silicon anodes. Reproduced with permission from ref. [16]. Copyright 2018, Elsevier.

In addition to lithium-silicate-based SEI derived from native oxide, another approach to directly deposit lithium silicates onto silicon as an artificial SEI can be implemented for superior battery anode performance. Zhu et al. synthesized a  $\text{Si@Li}_2\text{SiO}_3$  core-shell anode by oxidizing silicon nanoparticles at 600 °C in air with a subsequent thermal prelithiation process [53]. In comparison with the non-prelithiated  $\text{Si@SiO}_x$  anode,  $\text{Si@Li}_2\text{SiO}_3$  showed a much better initial Coulombic efficiency of 89.1% (vs. 66.5% in  $\text{Si@SiO}_x$  and 56.8% in Si), indicating prelithiation treatment can minimize irreversible Li-ion consumption during SEI formation reactions. Cycling tests also revealed that  $\text{Si@Li}_2\text{SiO}_3$  electrodes outperformed  $\text{Si@SiO}_x$  and Si not only in specific capacity but also in cycling stability. The  $\text{Li}_2\text{SiO}_3$  shell did slightly contribute to a charge/discharge capacity of 105.3/125.3 mA h g<sup>-1</sup>, which is consistent with the results of lithium activity discussed in the previous section [29]. The authors also demonstrated that the electron and Li-ion diffusion pathways of the  $\text{Li}_2\text{SiO}_3$  layer on the Si surface are better than those of the  $\text{SiO}_x$  layer by comparing their reaction resistances, leading to an outstanding rate capability [53].

Huang et al. utilized nanoporous nickel as the substrate to be coated with N-doped graphene (via CVD process), silicon (via magnetron sputtering), and hybrid silicate (via vapor deposition) to build a sandwiched N-doped graphene@Si@hybrid silicate (N-G@Si@HSi) nanoarchitecture [54]. Figure 9a shows the step-by-step details of the fabrication process of the bicontinuous porous material. A hybrid silicate was derived from the reactions of 3-mercaptopropyl trimethoxysilane (MPS), tetraethyl orthosilicate (TEOS) precursors, and

$\text{H}_2\text{O}$  vapors after a mild heating process. After the last nickel etching step, the free-standing film was used as the anode. The N-G@Si-30@HSi (Si-30: 59 nm silicon deposition thickness) exhibited extremely stable cycle performance among the other anode designs in Figure 9b. In the ingenious sandwiched anode design, the N-doped graphene serves as a flexible and conductive support, and the porous silicon nanolayer can avoid severe volume expansion and pulverization [6,55–61]. The amorphous external coating of hybrid lithium silicates plays an important role to significantly enhance the robustness and integrity of the structure and to facilitate the formation of stable SEI films [54].

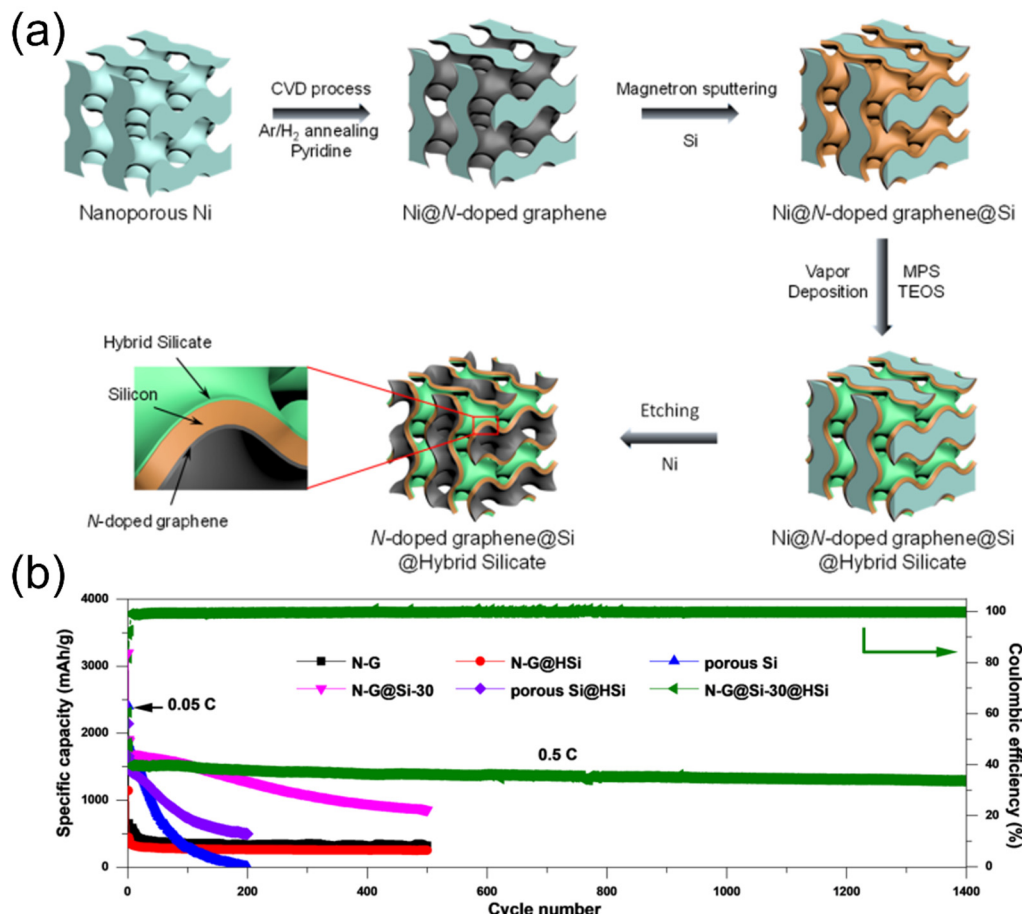


**Figure 9.** (a) Schematic drawing illustrating the fabrication process of the nanoporous N-G@Si@HSi anode. (b) Cycling performance of the N-G, N-G@HSi, porous Si, N-G@Si-30, porous Si@HSi, and N-G@Si-30@HSi electrodes at 0.05 C for the initial three cycles and at 0.5 C for the extended cycles. Reproduced with permission from ref. [54]. Copyright 2020, ACS Publications.

#### 4.2. Lithium Silicates in Lithium Metal Anodes

A Li<sub>4</sub>SiO<sub>4</sub> passivation layer can be formed on lithium metal anodes by in situ reactions between lithium foil and the a-SiO<sub>2</sub> thin film derived from electron cyclotron resonance (ECR)–chemical vapor deposition (CVD) [62]. Figure 10 exhibits the hierarchical structure of the composite lithium metal anode, which varies with a-SiO<sub>2</sub> deposition time, which is proportional to the thickness of the passivation layer. Without any interfacial protection, a rough surface was clearly found in the pristine lithium anode after lithiation (bottom left in Figure 10), and severe voltage polarization worsened with increasing cycle numbers due to significant degradation of the ether-based electrolyte [63]. While a-SiO<sub>2</sub> was deposited onto the lithium metal, a thin lithium silicide and lithiated silicon oxide bilayer was simultaneously generated by the immediate reactions with lithium. With a longer deposition time, pure a-SiO<sub>2</sub> started to exist on top of the bilayer, and the thickness of a-SiO<sub>2</sub> grew with the process time. After lithiation, the a-SiO<sub>2</sub> top layer was converted into Li<sub>4</sub>SiO<sub>4</sub>,

leading to a dendrite-free surface (SL-3 sample shown in the bottom of Figure 10), showing a flat plating/stripping voltage plateau with a minimal overpotential of 21.7 mV during repeated cycling, which represents excellent interfacial stability [62,64]. When the a-SiO<sub>2</sub> layer became too thick, not only ionically conductive Li<sub>4</sub>SiO<sub>4</sub> but also relatively insulating SiO was formed in the artificial top-layer structure, resulting in a higher overpotential due to the thicker protective layer's longer Li-ion migration distance and poorer diffusivity due to a higher SiO/Li<sub>4</sub>SiO<sub>4</sub> area ratio [62]. A few cracks were found in the lithium metal anode samples, particularly with a thicker a-SiO<sub>2</sub> protective layer, due to the heavy electrical stress induced by high electrical resistance, thereby leading to high interfacial resistance [62,65]. As a result, owing to higher Li-ion conductivity and Young's modulus (141.1 GPa) of Li<sub>4</sub>SiO<sub>4</sub> than those of a-SiO<sub>2</sub>, a carefully designed Li<sub>4</sub>SiO<sub>4</sub> artificial layer can serve as an excellent protective interface to stabilize the electrochemical reactions of lithium metal anodes [62].

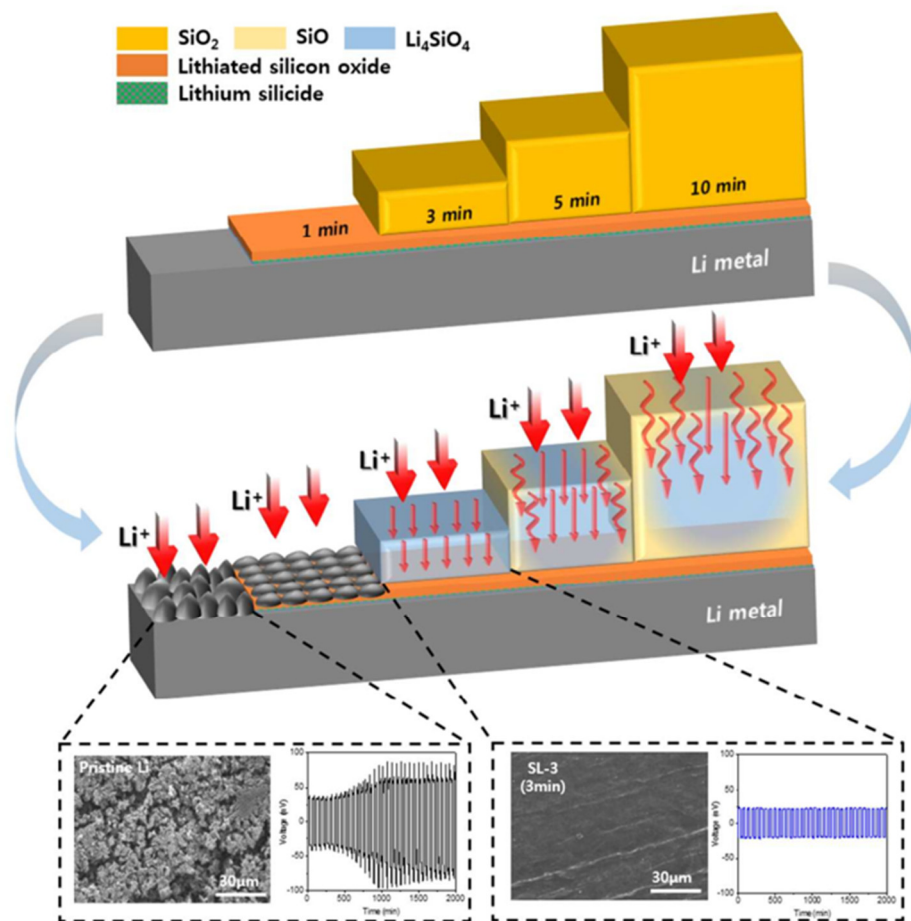


**Figure 10.** Schematic drawing illustrating the silicon oxide-based passivation layer deposited on the surface of lithium metal anode by the ECR-CVD method. Reproduced with permission from ref. [62]. Copyright 2018, ACS Publications.

A similar approach was developed by applying a-SiO<sub>2</sub> nanoparticles top of a lithium metal anode [66]. Silica spherical powders (200–300 nm in diameter) were sprayed onto a fresh lithium foil, followed by rolling-pressing to improve adherence. A compact and conformal SiO<sub>2</sub> layer with a thickness of 3.6  $\mu$ m then functioned as the artificial interfacial layer to stabilize the lithium-plating and stripping behaviors in lithium metal batteries (Figure 11a). The porous SiO<sub>2</sub> layer transformed into Li<sub>4</sub>SiO<sub>4</sub> after prelithiation, and zigzagged channels that can facilitate Li-ion transfer were formed between Li<sub>4</sub>SiO<sub>4</sub> particles. This protective film remained integrated after extended cycles, which guarantees low polarization (Figure 11b) and great cycle performance (Figure 11c). Unlike previously men-

tioned continuous a-SiO<sub>2</sub> film fabricated via the ECR-CVD method [62], a layer consisting of a-SiO<sub>2</sub> powder has plenty of interstices, where SEI species, such as LiF, can infiltrate during initial formation cycles [66]. This Li<sub>4</sub>SiO<sub>4</sub> hybrid structure possesses higher Young's modulus (up to 8.81 GPa), lower Li-ion diffusion barrier, and flexibility to accommodate volume expansion [66]. Therefore, great cyclability and rate performance originating from stable interfacial reactions and enhanced charge-transfer kinetics can be obtained.

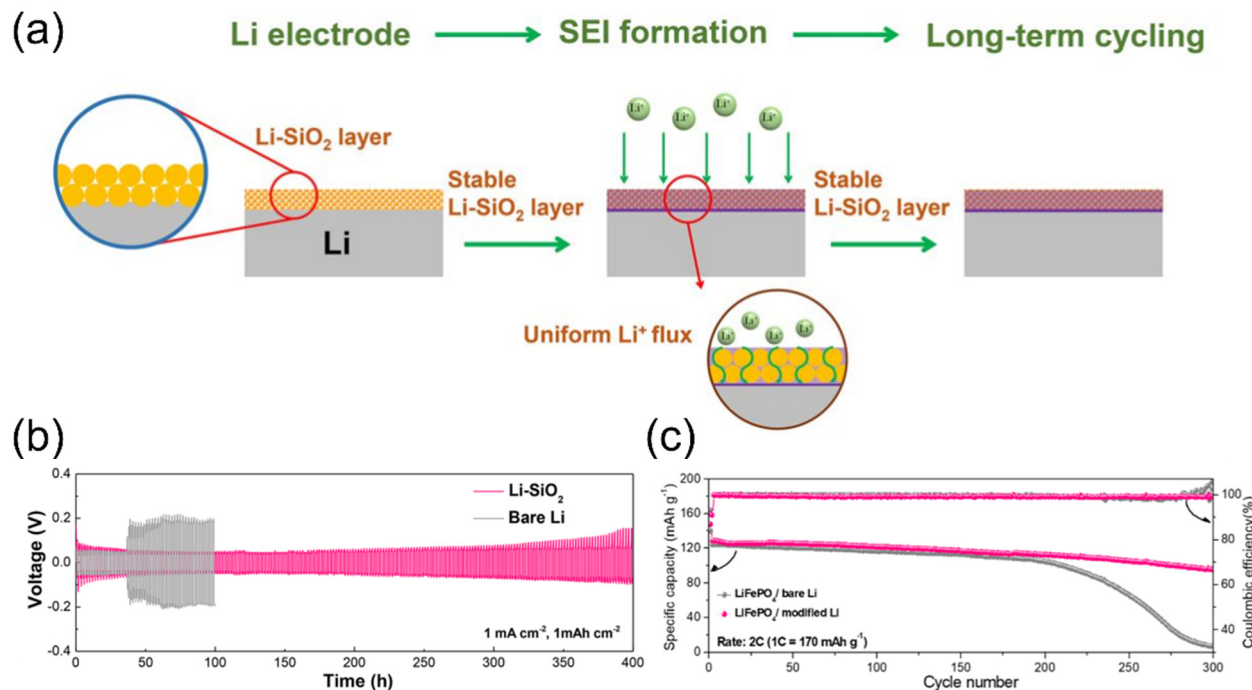


**Figure 11.** (a) Schematic drawing illustrating the fabrication of a conformal Li<sub>4</sub>SiO<sub>4</sub>-based hybrid layer for the dendrite-proof metallic lithium anode. (b) Electrochemical cycling stability of bare Li and modified Li symmetric cells ( $1 \text{ mA cm}^{-2}$ ,  $1 \text{ mA h cm}^{-2}$ ). (c) Long-term cycling performance of Li metal full cells. Reproduced with permission from ref. [66]. Copyright 2020, ACS Publications.

Liu et al. directly exposed a piece of lithium foil to MPS and TEOS vapors, and lithium silicates ( $\text{Li}_x\text{Si}_y\text{O}_z$ ) were formed and bound with surface  $\text{Li}_2\text{O}$  and  $\text{LiOH}$ , which were naturally generated on the lithium metal before vapor deposition [67]. It was reported that when the hydroxyl group on lithium reacts with TEOS, the protective film formed *in situ* possesses a self-healing feature that can dynamically repair the corroded metallic lithium anode, which, remarkably, improves its reversibility [68]. Since MPS and TEOS are both organosilicon compounds, methoxysilane ( $-\text{Si}-\text{OCH}_3$ , from MPS) and ethoxysilane ( $-\text{Si}-\text{OCH}_2\text{CH}_3$ , from TEOS) can undergo hydrolysis and condensation reactions to create a hybrid organic–inorganic lithium silicate layer comprising a “soft” organic moiety (mercaptopropyl groups) and a “hard” inorganic moiety (lithium silicates) [67]. The soft part in the artificial layer can improve flexibility and robustness, and the hard part can enhance Li-ion transport and block the growth of lithium dendrite. Both organic and inorganic structures synergistically stabilize anode reactions of lithium metal during charge and discharge, leading to great cycle life in Li–LiFePO<sub>4</sub> and Li–S full cells [67]. Ju et al. adopted aluminum silicate fibers to protect lithium metal anodes, realizing dendrite-free lithium anode reactions and a fast Li-ion conducting interface [69]. Inorganic species of lithium aluminates ( $\text{Li}_x\text{AlO}_y$ ) and lithium silicates ( $\text{Li}_x\text{SiO}_y$ ) were detected upon cycling, implying alternative metal silicates could also be used as precursors of artificial SEI for lithium metal anodes.

Liang et al. floated lithium metal foil on a solution of 3-glycidyloxypropyltrimethoxysilane (GPTMS) and LiOH, and Li<sub>6</sub>Si<sub>2</sub>O<sub>7</sub> particles were adaptively embedded in the Si–O–Si

polymer as a protective dual-phase layer during the initial lithium-stripping/plating process [70]. This dual-phase interface showed high elastic modulus, high mechanical rigidity, and high interface energy, which can suppress the formation of one-dimensional lithium dendrite whiskers [71]. Moreover, the structure of the composite shielding layer can efficiently lower the Li-ion migration barrier [72]. An Li–air battery with an adaptive polymer-inorganic hybrid structure on the lithium metal anode can perform up to 180 cycles in an air atmosphere (25 °C, 15% humidity) with a capacity limitation of 1000 mAh g<sup>-1</sup> under a high current density of 1000 mA g<sup>-1</sup> [70]. Yu et al. employed the self-healing protective film concept by not only treating lithium metal foil in TEOS as the anode but using TEOS as an additive in the electrolyte for film-forming purposes during cycling [68]. A thin lithium silicate layer can be formed under the reaction between TEOS and the detrimental corrosion products LiOH on the surface of lithium metal anodes in the highly corrosive environment of Li–O<sub>2</sub> batteries. The shielded lithium metal anode with film-forming electrolyte additive gives Li–O<sub>2</sub> batteries a considerable boost in cycle life (up to 144 cycles), indicating great dynamic-repair capability of the protective layer on the lithium metal anode [68].

Lithium silicates can also be used to serve as a bridge layer between lithium metal anodes and solid-state electrolytes to lower the interfacial resistance. To achieve a low interfacial resistance with lithium metal of the garnet solid electrolyte, an amorphous Li<sub>2</sub>SiO<sub>3</sub> interlayer was proposed [73]. A liquid-phase coating process was utilized to deposit a thin lithium silicate film on the surface of garnet solid electrolytes, followed by a heat treatment, and metallic lithium was directly pressed onto the modified surface. This approach achieved stable cycling performance and a low interfacial resistance of 44 Ω cm<sup>2</sup>, which was more than 10 times lower than that of the uncoated solid electrolyte. The authors proposed a possible reaction mechanism whereby Li<sub>2</sub>SiO<sub>3</sub> decomposed into Li<sub>21</sub>Si<sub>5</sub> and Li<sub>2</sub>O after being in contact with lithium metal [73].

To sum up, there are many approaches using lithium silicates with various Li/Si ratios to improve anode performance in Li-ion and Li metal batteries. The majority of previous research focused on the Li<sub>4</sub>SiO<sub>4</sub> protective coating on silicon and metallic lithium anodes. With a rational design of composite anode structure, unwanted interfacial reactions can be either suppressed or eliminated, leading to better performance of long cycle life and small overpotential. The swelling issue of Si-based anodes can be addressed by utilizing SiO anodes where lithium silicates are formed in situ during cell formation or by adopting a 3D framework to accommodate lithium silicate-protected silicon. Table 1 summarizes the previous works employing lithium silicates to boost battery anode performance. The studies related to modified metallic lithium anodes utilized excess lithium in the full cell. Without detailed full-cell design parameters, their specific capacity cannot be confirmed at this point. Still, other lithium silicate phases, such as Li<sub>2</sub>Si<sub>2</sub>O<sub>5</sub> and Li<sub>6</sub>Si<sub>2</sub>O<sub>7</sub>, have yet to be identified as a good anode-protection-layer material, like Li<sub>4</sub>SiO<sub>4</sub> and Li<sub>2</sub>SiO<sub>3</sub>. As a result, additional in-depth research is required before a sound judgment can be reached.

**Table 1.** Electrochemical performance of anode materials protected by lithium silicates.

Anode Material	Lithium Silicate Phase	Strategy	Capacity (mAh g <sup>-1</sup> )	C Rate	Cycle Number	Capacity Retention	Reference
Graphite	Li <sub>2</sub> SiO <sub>3</sub>	Co-modified with Li <sub>2</sub> CO <sub>3</sub>	371	1 C	50	96.2%	[30]
Li <sub>4</sub> Ti <sub>5</sub> O <sub>12</sub>	Li <sub>2</sub> SiO <sub>3</sub>	Supported by graphene	463	~0.3 C	200	89.1%	[31]
Si	Li <sub>2</sub> SiO <sub>3</sub>	Core-shell structure	3201	~1 C	1000	39%	[53]
Li	Li <sub>4</sub> SiO <sub>4</sub>	Lithiating a-SiO <sub>2</sub> coating	Excess Li	0.5 C	100	73.4%	[62]
Li	Li <sub>4</sub> SiO <sub>4</sub>	Lithiating nano a-SiO <sub>2</sub>	Excess Li	2 C	300	74%	[66]
Li	Li <sub>x</sub> SiO <sub>y</sub>	Lithiating organosilicons	Excess Li	0.3 C	300	~60%	[67]
Li	Li <sub>2</sub> SiO <sub>3</sub>	Reducing interfacial resistance between Li/SSE	Excess Li	0.18 C	100	~82%	[73]

## 5. Summary and Outlook

The properties of various lithium silicate phases have been carefully reviewed in this paper.  $\text{Li}_4\text{SiO}_4$ , regarded as the major compound among lithiated  $\text{SiO}$  anodes and SEI deposited on the naturally oxidized surface of Si anodes, is the most investigated lithium silicate material in battery applications.  $\text{Li}_4\text{SiO}_4$  and  $\text{Li}_2\text{SiO}_3$  are frequently used to protect high-capacity silicon and lithium metal anodes.  $\text{Li}_2\text{Si}_2\text{O}_5$  and  $\text{Li}_6\text{Si}_2\text{O}_7$  can also be found in some  $\text{SiO}_x$ -based battery anodes after the lithiation process or during charge/discharge reactions. In general, lithium silicates play an important role in anodes for (1) stabilization of interfacial reactions, (2) buffering of volume expansion without any mechanical failure, and (3) offering fast Li-ion transportation pathways. Further systematic research is required to determine which lithium silicate phase is the best in class to protect silicon and lithium anode materials.

Lithium silicates can be synthesized by lithiation of amorphous silica or organosilicon compounds. The necessary raw materials are commonly seen in chemical engineering and semiconductor industries and are low-cost and easy to process, making this approach feasible and scalable for battery anode applications. A streamlined manufacturing process needs to be developed for better integration into current battery-production procedures. Aside from the success of  $\text{SiO}/\text{SiO}_x$  anode materials, lithium silicates have now been successfully adopted in high-capacity anode systems, especially serving as the major ingredient in the protection layer of metallic lithium. Alternative lithium metal oxide compounds could be developed if comparable ionic and mechanical properties can be obtained. Due to the rigid nature of ceramics-like oxide-based ion-conducting materials that might lose intimate contact with the active anode material during cycling, a polymer-inorganic (soft-rigid) hybrid protection layer appears to be a promising option for achieving both high elasticity and ionic conductivity to shield silicon and lithium metal anodes [67,70].

Currently, the lithium silicates adopted in commercial battery systems are mostly formed during the lithiation process of  $\text{SiO}$  anodes at the formation step of battery-cell manufacturing. The challenges of lithium silicate-enhanced anodes are: (1) The efficacy of anode protection by lithium silicates synthesized from silica or other organosilicon compounds other than  $\text{SiO}$  is still not clear at the industry level; (2) The processing and preparation of lithium silicate protective layers could be cost-ineffective; (3) The long-term protection and adhesion stability of lithium silicates in integrated anodes is unknown. Strategies concerning smart architectural designs, innovative methods of anode integration processes, low-cost and scalable synthesis, and long-cycle durability improvements will need to be thoroughly investigated before lithium silicates can be widely applied in various anode systems for practical Li-ion and Li metal batteries.

**Author Contributions:** Y.-S.S. drafted the majority of this review paper. K.-C.H., P.S. and J.-Y.H. were involved in the editing and literature-screening efforts. All authors participated in writing the manuscript and discussing the contents to be included in this review. All authors have read and agreed to the published version of the manuscript.

**Funding:** This research was funded by the Ministry of Science and Technology (MOST) of Taiwan (110-2113-M-A49-027-MY2) and by the Ministry of Education (MOE) of Taiwan under the Yushan Young Scholar Program (110B53-8) and the Higher Education SPROUT Project of the National Yang Ming Chiao Tung University (110W266).

**Institutional Review Board Statement:** Not applicable.

**Informed Consent Statement:** Not applicable.

**Data Availability Statement:** All collected data are presented in the manuscript.

**Conflicts of Interest:** The authors declare no conflict of interest.

## References

- Yamamura, H.; Nobuhara, K.; Nakanishi, S.; Iba, H.; Okada, S. Investigation of the Irreversible Reaction Mechanism and the Reactive Trigger on SiO Anode Material for Lithium-Ion Battery. *J. Ceram. Soc. Jpn.* **2011**, *119*, 855–860. [[CrossRef](#)]
- Zhang, Y.; Guo, G.; Chen, C.; Jiao, Y.; Li, T.; Chen, X.; Yang, Y.; Yang, D.; Dong, A. An Affordable Manufacturing Method to Boost the Initial Coulombic Efficiency of Disproportionated SiO Lithium-Ion Battery Anodes. *J. Power Sources* **2019**, *426*, 116–123. [[CrossRef](#)]
- Hohl, A.; Wieder, T.; van Aken, P.A.; Weirich, T.E.; Denninger, G.; Vidal, M.; Oswald, S.; Deneke, C.; Mayer, J.; Fuess, H. An Interface Clusters Mixture Model for the Structure of Amorphous Silicon Monoxide (SiO). *J. Non-Cryst. Solids* **2003**, *320*, 255–280. [[CrossRef](#)]
- Kim, J.-H.; Park, C.-M.; Kim, H.; Kim, Y.-J.; Sohn, H.-J. Electrochemical Behavior of SiO Anode for Li Secondary Batteries. *J. Electroanal. Chem.* **2011**, *661*, 245–249. [[CrossRef](#)]
- Chen, T.; Wu, J.; Zhang, Q.; Su, X. Recent Advancement of SiO<sub>x</sub> Based Anodes for Lithium-Ion Batteries. *J. Power Sources* **2017**, *363*, 126–144. [[CrossRef](#)]
- Liu, X.H.; Zhong, L.; Huang, S.; Mao, S.X.; Zhu, T.; Huang, J.Y. Size-Dependent Fracture of Silicon Nanoparticles During Lithiation. *ACS Nano* **2012**, *6*, 1522–1531. [[CrossRef](#)] [[PubMed](#)]
- Jin, Y.; Zhu, B.; Lu, Z.; Liu, N.; Zhu, J. Challenges and Recent Progress in the Development of Si Anodes for Lithium-Ion Battery. *Adv. Energy Mater.* **2017**, *7*, 1700715. [[CrossRef](#)]
- Gu, M.; He, Y.; Zheng, J.; Wang, C. Nanoscale Silicon as Anode for Li-Ion Batteries: The Fundamentals, Promises, and Challenges. *Nano Energy* **2015**, *17*, 366–383. [[CrossRef](#)]
- Pan, K.; Zou, F.; Canova, M.; Zhu, Y.; Kim, J.-H. Systematic Electrochemical Characterizations of Si and SiO Anodes for High-Capacity Li-Ion Batteries. *J. Power Sources* **2019**, *413*, 20–28. [[CrossRef](#)]
- Hirata, A.; Kohara, S.; Asada, T.; Arao, M.; Yogi, C.; Imai, H.; Tan, Y.; Fujita, T.; Chen, M. Atomic-Scale Disproportionation in Amorphous Silicon Monoxide. *Nat. Commun.* **2016**, *7*, 11591. [[CrossRef](#)] [[PubMed](#)]
- Liu, Z.; Yu, Q.; Zhao, Y.; He, R.; Xu, M.; Feng, S.; Li, S.; Zhou, L.; Mai, L. Silicon Oxides: A Promising Family of Anode Materials for Lithium-Ion Batteries. *Chem. Soc. Rev.* **2019**, *48*, 285–309. [[CrossRef](#)] [[PubMed](#)]
- Choi, I.; Lee, M.J.; Oh, S.M.; Kim, J.J. Fading Mechanisms of Carbon-Coated and Disproportionated Si/SiO<sub>x</sub> Negative Electrode (Si/SiO<sub>x</sub>/C) in Li-Ion Secondary Batteries: Dynamics and Component Analysis by TEM. *Electrochim. Acta* **2012**, *85*, 369–376. [[CrossRef](#)]
- Jung, S.C.; Kim, H.-J.; Kim, J.-H.; Han, Y.-K. Atomic-Level Understanding toward a High-Capacity and High-Power Silicon Oxide (SiO) Material. *J. Phys. Chem. C* **2016**, *120*, 886–892. [[CrossRef](#)]
- Sivonxay, E.; Aykol, M.; Persson, K.A. The Lithiation Process and Li Diffusion in Amorphous SiO<sub>2</sub> and Si from First-Principles. *Electrochim. Acta* **2020**, *331*, 135344. [[CrossRef](#)]
- Reynier, Y.; Vincens, C.; Leys, C.; Amestoy, B.; Mayousse, E.; Chavillon, B.; Blanc, L.; Gutel, E.; Porcher, W.; Hirose, T.; et al. Practical Implementation of Li Doped SiO in High Energy Density 21700 Cell. *J. Power Sources* **2020**, *450*, 227699. [[CrossRef](#)]
- Cao, C.; Abate, I.I.; Sivonxay, E.; Shyam, B.; Jia, C.; Moritz, B.; Devereaux, T.P.; Persson, K.A.; Steinrück, H.-G.; Toney, M.F. Solid Electrolyte Interphase on Native Oxide-Terminated Silicon Anodes for Li-Ion Batteries. *Joule* **2019**, *3*, 762–781. [[CrossRef](#)]
- Hirose, T.; Morishita, M.; Yoshitake, H.; Sakai, T. Study of Structural Changes That Occurred during Charge/Discharge of Carbon-Coated SiO Anode by Nuclear Magnetic Resonance. *Solid State Ion.* **2017**, *303*, 154–160. [[CrossRef](#)]
- Liu, Y.; Wu, Y.; Zheng, J.; Wang, Y.; Ju, Z.; Lu, G.; Sheng, O.; Nai, J.; Liu, T.; Zhang, W.; et al. Silicious Nanowires Enabled Dendrites Suppression and Flame Retardancy for Advanced Lithium Metal Anodes. *Nano Energy* **2021**, *82*, 105723. [[CrossRef](#)]
- Yu, B.-C.; Hwa, Y.; Kim, J.-H.; Sohn, H.-J. A New Approach to Synthesis of Porous SiO<sub>x</sub> Anode for Li-Ion Batteries via Chemical Etching of Si Crystallites. *Electrochim. Acta* **2014**, *117*, 426–430. [[CrossRef](#)]
- Yu, B.-C.; Hwa, Y.; Park, C.-M.; Sohn, H.-J. Reaction Mechanism and Enhancement of Cyclability of SiO Anodes by Surface Etching with NaOH for Li-Ion Batteries. *J. Mater. Chem. A* **2013**, *1*, 4820. [[CrossRef](#)]
- Hirose, T.; Morishita, M.; Yoshitake, H.; Sakai, T. Investigation of Carbon-Coated SiO Phase Changes during Charge/Discharge by X-Ray Absorption Fine Structure. *Solid State Ion.* **2017**, *304*, 1–6. [[CrossRef](#)]
- Coyle, J.; Apblett, C.; Brumbach, M.; Ohlhausen, J.; Stoldt, C. Structural and Compositional Characterization of RF Magnetron Cospattered Lithium Silicate Films: From Li<sub>2</sub>Si<sub>2</sub>O<sub>5</sub> to Lithium-Rich Li<sub>8</sub>SiO<sub>6</sub>. *J. Vac. Sci. Technol. A* **2017**, *35*, 061509. [[CrossRef](#)]
- Philippe, B.; Dedryvère, R.; Allouche, J.; Lindgren, F.; Gorgoi, M.; Rensmo, H.; Gonbeau, D.; Edström, K. Nanosilicon Electrodes for Lithium-Ion Batteries: Interfacial Mechanisms Studied by Hard and Soft X-Ray Photoelectron Spectroscopy. *Chem. Mater.* **2012**, *24*, 1107–1115. [[CrossRef](#)]
- Chang, W.-S.; Park, C.-M.; Kim, J.-H.; Kim, Y.-U.; Jeong, G.; Sohn, H.-J. Quartz (SiO<sub>2</sub>): A New Energy Storage Anode Material for Li-Ion Batteries. *Energy Environ. Sci.* **2012**, *5*, 6895. [[CrossRef](#)]
- Veluchamy, A.; Doh, C.-H.; Kim, D.-H.; Lee, J.-H.; Lee, D.-J.; Ha, K.-H.; Shin, H.-M.; Jin, B.-S.; Kim, H.-S.; Moon, S.-I.; et al. Improvement of Cycle Behaviour of SiO/C Anode Composite by Thermochemically Generated Li<sub>4</sub>SiO<sub>4</sub> Inert Phase for Lithium Batteries. *J. Power Sources* **2009**, *188*, 574–577. [[CrossRef](#)]
- Doh, C.-H.; Veluchamy, A.; Oh, M.-W.; Han, B.-C. Analysis on the Formation of Li<sub>4</sub>SiO<sub>4</sub> and Li<sub>2</sub>SiO<sub>3</sub> through First Principle Calculations and Comparing with Experimental Data Related to Lithium Battery. *J. Electrochem. Sci. Technol.* **2011**, *2*, 146–151. [[CrossRef](#)]

27. Gong, Y.; Yu, X.; Yang, M.; Wei, J.; Shi, Y.; Huang, Z.; Lu, T.; Huang, W. A Facile Approach to Fabricate Li<sub>4</sub>SiO<sub>4</sub> Ceramic Pebbles as Tritium Breeding Materials. *Mater. Lett.* **2015**, *159*, 245–248. [CrossRef]
28. Wang, K.; Yin, Z.; Zhao, P. Synthesis of Macroporous Li<sub>4</sub>SiO<sub>4</sub> via a Citric Acid-Based Sol–Gel Route Coupled with Carbon Coating and Its CO<sub>2</sub> Chemisorption Properties. *Ceram. Int.* **2016**, *42*, 2990–2999. [CrossRef]
29. Yang, S.; Wang, Q.; Miao, J.; Zhang, D.; Chen, Y.; Yang, H. Synthesis of Graphene Supported Li<sub>2</sub>SiO<sub>3</sub> as a High Performance Anode Material for Lithium-Ion Batteries. *Appl. Surf. Sci.* **2018**, *444*, 522–529. [CrossRef]
30. Xiao, Y.; Wang, G.; Zhou, S.; Sun, Y.; Zhao, Q.; Gong, Y.; Lu, T.; Luo, C.; Yan, K. Enhanced Electrochemical Performance and Decreased Strain of Graphite Anode by Li<sub>2</sub>SiO<sub>3</sub> and Li<sub>2</sub>CO<sub>3</sub> Co-Modifying. *Electrochim. Acta* **2017**, *223*, 8–20. [CrossRef]
31. Wang, Q.; Yang, S.; Miao, J.; Lu, M.; Wen, T.; Sun, J. Graphene Supported Li<sub>2</sub>SiO<sub>3</sub>/Li<sub>4</sub>Ti<sub>5</sub>O<sub>12</sub> Nanocomposites with Improved Electrochemical Performance as Anode Material for Lithium-Ion Batteries. *Appl. Surf. Sci.* **2017**, *403*, 635–644. [CrossRef]
32. Wang, Q.; Yang, S.; Miao, J.; Zhang, Y.; Zhang, D.; Chen, Y.; Li, Z. Synthesis of Graphene Supported Li<sub>2</sub>SiO<sub>3</sub>/Li<sub>2</sub>SnO<sub>3</sub> Anode Material for Rechargeable Lithium Ion Batteries. *Appl. Surf. Sci.* **2019**, *469*, 253–261. [CrossRef]
33. Yom, J.H.; Hwang, S.W.; Cho, S.M.; Yoon, W.Y. Improvement of Irreversible Behavior of SiO Anodes for Lithium Ion Batteries by a Solid State Reaction at High Temperature. *J. Power Sources* **2016**, *311*, 159–166. [CrossRef]
34. Yan, M.-Y.; Li, G.; Zhang, J.; Tian, Y.-F.; Yin, Y.-X.; Zhang, C.-J.; Jiang, K.-C.; Xu, Q.; Li, H.-L.; Guo, Y.-G. Enabling SiO<sub>x</sub>/C Anode with High Initial Coulombic Efficiency through a Chemical Pre-Lithiation Strategy for High-Energy-Density Lithium-Ion Batteries. *ACS Appl. Mater. Interfaces* **2020**, *12*, 27202–27209. [CrossRef] [PubMed]
35. Alemi, A.; Khademinia, S.; Sertkol, M. Part III: Lithium Metasilicate (Li<sub>2</sub>SiO<sub>3</sub>)—Mild Condition Hydrothermal Synthesis, Characterization and Optical Properties. *Int. Nano Lett.* **2015**, *5*, 77–83. [CrossRef]
36. Wu, X.; Wen, Z.; Xu, X.; Wang, X.; Lin, J. Synthesis and Characterization of Li<sub>4</sub>SiO<sub>4</sub> Nano-Powders by a Water-Based Sol-Gel Process. *J. Nucl. Mater.* **2009**, *392*, 471–475. [CrossRef]
37. Li, M.; Zeng, Y.; Ren, Y.; Zeng, C.; Gu, J.; Feng, X.; He, H. Fabrication and Lithium Storage Performance of Sugar Apple-Shaped SiO<sub>x</sub>@C Nanocomposite Spheres. *J. Power Sources* **2015**, *288*, 53–61. [CrossRef]
38. Sun, Q.; Zhang, B.; Fu, Z.-W. Lithium Electrochemistry of SiO<sub>2</sub> Thin Film Electrode for Lithium-Ion Batteries. *Appl. Surf. Sci.* **2008**, *254*, 3774–3779. [CrossRef]
39. Lener, G.; Otero, M.; Barraco, D.E.; Leiva, E.P.M. Energetics of Silica Lithiation and Its Applications to Lithium Ion Batteries. *Electrochim. Acta* **2018**, *259*, 1053–1058. [CrossRef]
40. Alemi, A.; Khademinia, S.; Sertkol, M. Lithium Disilicate (Li<sub>2</sub>Si<sub>2</sub>O<sub>5</sub>): Mild Condition Hydrothermal Synthesis, Characterization and Optical Properties. *J. Nanostruct.* **2014**, *4*, 407–412.
41. Koroleva, O.N.; Shtenberg, M.V.; Khvorov, P.V. Vibrational Spectroscopic and X-Ray Diffraction Study of Crystalline Phases in the Li<sub>2</sub>O-SiO<sub>2</sub> System. *Russ. J. Inorg. Chem.* **2014**, *59*, 255–258. [CrossRef]
42. Wang, Y.T.; Cao, Y.D.; Hu, J.; Zhang, W.J.; Wu, D.P.; Shen, L. Fabrication of Lithium Silicate Doped with Lithium Titanate by Solid-State Reaction and Its XRD Study. *AMR* **2012**, *624*, 200–203. [CrossRef]
43. Prihandoko, B.; Sardjono, P.; Zulfia, A.; Siradj, E. The effect of Li<sub>2</sub>O on composite LTAP and windows glasses. *Indones. J. Mater. Sci.* **2007**, *9*, 6.
44. Piazza, G.; Reimann, J.; Günther, E.; Knitter, R.; Roux, N.; Lulewicz, J.D. Behaviour of Ceramic Breeder Materials in Long Time Annealing Experiments. *Fusion Eng. Des.* **2001**, *58–59*, 653–659. [CrossRef]
45. Su, X.; Wu, Q.; Li, J.; Xiao, X.; Lott, A.; Lu, W.; Sheldon, B.W.; Wu, J. Silicon-Based Nanomaterials for Lithium-Ion Batteries: A Review. *Adv. Energy Mater.* **2014**, *4*, 1300882. [CrossRef]
46. Zuo, X.; Zhu, J.; Müller-Buschbaum, P.; Cheng, Y.-J. Silicon Based Lithium-Ion Battery Anodes: A Chronicle Perspective Review. *Nano Energy* **2017**, *31*, 113–143. [CrossRef]
47. Cheng, X.-B.; Zhang, R.; Zhao, C.-Z.; Zhang, Q. Toward Safe Lithium Metal Anode in Rechargeable Batteries: A Review. *Chem. Rev.* **2017**, *117*, 10403–10473. [CrossRef]
48. Lin, D.; Liu, Y.; Cui, Y. Reviving the Lithium Metal Anode for High-Energy Batteries. *Nat. Nanotech.* **2017**, *12*, 194–206. [CrossRef]
49. Cheng, X.-B.; Zhang, R.; Zhao, C.-Z.; Wei, F.; Zhang, J.-G.; Zhang, Q. A Review of Solid Electrolyte Interphases on Lithium Metal Anode. *Adv. Sci.* **2016**, *3*, 1500213. [CrossRef]
50. Philippe, B.; Dedryvère, R.; Gorgoi, M.; Rensmo, H.; Gonbeau, D.; Edström, K. Improved Performances of Nanosilicon Electrodes Using the Salt LiFSI: A Photoelectron Spectroscopy Study. *J. Am. Chem. Soc.* **2013**, *135*, 9829–9842. [CrossRef]
51. Schroder, K.W.; Celio, H.; Webb, L.J.; Stevenson, K.J. Examining Solid Electrolyte Interphase Formation on Crystalline Silicon Electrodes: Influence of Electrochemical Preparation and Ambient Exposure Conditions. *J. Phys. Chem. C* **2012**, *116*, 19737–19747. [CrossRef]
52. Xiong, J.; Yang, J.; Wang, G.; Saeed, T.; Liu, Y.; Kaczmarek, S.E.; Lu, W.; Wu, Q. Investigations on the Effect of Current Density on SiO/Si Composite Electrodes. *Electrochim. Acta* **2021**, *393*, 139072. [CrossRef]
53. Zhu, Y.; Hu, W.; Zhou, J.; Cai, W.; Lu, Y.; Liang, J.; Li, X.; Zhu, S.; Fu, Q.; Qian, Y. Prelithiated Surface Oxide Layer Enabled High-Performance Si Anode for Lithium Storage. *ACS Appl. Mater. Interfaces* **2019**, *11*, 18305–18312. [CrossRef]
54. Huang, G.; Han, J.; Lu, Z.; Wei, D.; Kashani, H.; Watanabe, K.; Chen, M. Ultrastable Silicon Anode by Three-Dimensional Nanoarchitecture Design. *ACS Nano* **2020**, *14*, 4374–4382. [CrossRef] [PubMed]
55. An, W.; Gao, B.; Mei, S.; Xiang, B.; Fu, J.; Wang, L.; Zhang, Q.; Chu, P.K.; Huo, K. Scalable Synthesis of Ant-Nest-like Bulk Porous Silicon for High-Performance Lithium-Ion Battery Anodes. *Nat. Commun.* **2019**, *10*, 1447. [CrossRef]

56. Ge, M.; Fang, X.; Rong, J.; Zhou, C. Review of Porous Silicon Preparation and Its Application for Lithium-Ion Battery Anodes. *Nanotechnology* **2013**, *24*, 422001. [CrossRef]
57. Ge, M.; Rong, J.; Fang, X.; Zhang, A.; Lu, Y.; Zhou, C. Scalable Preparation of Porous Silicon Nanoparticles and Their Application for Lithium-Ion Battery Anodes. *Nano Res.* **2013**, *6*, 174–181. [CrossRef]
58. Ge, M.; Rong, J.; Fang, X.; Zhou, C. Porous Doped Silicon Nanowires for Lithium Ion Battery Anode with Long Cycle Life. *Nano Lett.* **2012**, *12*, 2318–2323. [CrossRef]
59. Jia, H.; Zheng, J.; Song, J.; Luo, L.; Yi, R.; Estevez, L.; Zhao, W.; Patel, R.; Li, X.; Zhang, J.-G. A Novel Approach to Synthesize Micrometer-Sized Porous Silicon as a High Performance Anode for Lithium-Ion Batteries. *Nano Energy* **2018**, *50*, 589–597. [CrossRef]
60. Xiao, Q.; Gu, M.; Yang, H.; Li, B.; Zhang, C.; Liu, Y.; Liu, F.; Dai, F.; Yang, L.; Liu, Z.; et al. Inward Lithium-Ion Breathing of Hierarchically Porous Silicon Anodes. *Nat. Commun.* **2015**, *6*, 8844. [CrossRef] [PubMed]
61. Zhao, Y.; Liu, X.; Li, H.; Zhai, T.; Zhou, H. Hierarchical Micro/Nano Porous Silicon Li-Ion Battery Anodes. *Chem. Commun.* **2012**, *48*, 5079. [CrossRef]
62. Kim, J.Y.; Kim, A.-Y.; Liu, G.; Woo, J.-Y.; Kim, H.; Lee, J.K. Li<sub>4</sub>SiO<sub>4</sub>-Based Artificial Passivation Thin Film for Improving Interfacial Stability of Li Metal Anodes. *ACS Appl. Mater. Interfaces* **2018**, *10*, 8692–8701. [CrossRef] [PubMed]
63. Bieker, G.; Winter, M.; Bieker, P. Electrochemical in Situ Investigations of SEI and Dendrite Formation on the Lithium Metal Anode. *Phys. Chem. Chem. Phys.* **2015**, *17*, 8670–8679. [CrossRef]
64. Kang, H.-K.; Woo, S.-G.; Kim, J.-H.; Lee, S.-R.; Kim, Y.-J. Conductive Porous Carbon Film as a Lithium Metal Storage Medium. *Electrochim. Acta* **2015**, *176*, 172–178. [CrossRef]
65. Kuo, D.-H.; Yang, D.-G. Thick SiO<sub>2</sub> Films Obtained by Plasma-Enhanced Chemical Vapor Deposition Using Hexamethyldisilazane, Carbon Dioxide, and Hydrogen. *J. Electrochem. Soc.* **2000**, *147*, 2679. [CrossRef]
66. Yuan, Y.; Wu, F.; Liu, Y.; Wang, X.; Zhang, K.; Zheng, L.; Wang, Z.; Bai, Y.; Wu, C. Rational Tuning of a Li<sub>4</sub>SiO<sub>4</sub>-Based Hybrid Interface with Unique Stepwise Prelithiation for Dendrite-Proof and High-Rate Lithium Anodes. *ACS Appl. Mater. Interfaces* **2020**, *12*, 39362–39371. [CrossRef]
67. Liu, F.; Xiao, Q.; Wu, H.B.; Shen, L.; Xu, D.; Cai, M.; Lu, Y. Fabrication of Hybrid Silicate Coatings by a Simple Vapor Deposition Method for Lithium Metal Anodes. *Adv. Energy Mater.* **2018**, *8*, 1701744. [CrossRef]
68. Yu, Y.; Yin, Y.-B.; Ma, J.-L.; Chang, Z.-W.; Sun, T.; Zhu, Y.-H.; Yang, X.-Y.; Liu, T.; Zhang, X.-B. Designing a Self-Healing Protective Film on a Lithium Metal Anode for Long-Cycle-Life Lithium-Oxygen Batteries. *Energy Storage Mater.* **2019**, *18*, 382–388. [CrossRef]
69. Ju, Z.; Jin, C.; Yuan, H.; Yang, T.; Sheng, O.; Liu, T.; Liu, Y.; Wang, Y.; Ma, F.; Zhang, W.; et al. A Fast-Ion Conducting Interface Enabled by Aluminum Silicate Fibers for Stable Li Metal Batteries. *Chem. Eng. J.* **2021**, *408*, 128016. [CrossRef]
70. Liang, W.; Lian, F.; Meng, N.; Lu, J.; Ma, L.; Zhao, C.-Z.; Zhang, Q. Adaptive Formed Dual-Phase Interface for Highly Durable Lithium Metal Anode in Lithium-Air Batteries. *Energy Storage Mater.* **2020**, *28*, 350–356. [CrossRef]
71. Stone, G.M.; Mullin, S.A.; Teran, A.A.; Hallinan, D.T.; Minor, A.M.; Hexemer, A.; Balsara, N.P. Resolution of the Modulus versus Adhesion Dilemma in Solid Polymer Electrolytes for Rechargeable Lithium Metal Batteries. *J. Electrochem. Soc.* **2012**, *159*, A222–A227. [CrossRef]
72. Croce, F.; Appetecchi, G.B.; Persi, L.; Scrosati, B. Nanocomposite Polymer Electrolytes for Lithium Batteries. *Nature* **1998**, *394*, 456–458. [CrossRef]
73. Rosero-Navarro, N.C.; Kajiura, R.; Jalem, R.; Tateyama, Y.; Miura, A.; Tadanaga, K. Significant Reduction in the Interfacial Resistance of Garnet-Type Solid Electrolyte and Lithium Metal by a Thick Amorphous Lithium Silicate Layer. *ACS Appl. Energy Mater.* **2020**, *3*, 5533–5541. [CrossRef]